JMEPEG (2004) 13:287-294
DOI: 10.1361/10599490419261


1059-9495/$19.00

# Observations on the Structural Degradation of Silver During Simultaneous Exposure to Oxidizing and Reducing Environments

*Prabhakar Singh, Zhenguo Yang, Vish Viswanathan, and Jeff W. Stevenson*

*(Submitted 12 November 2003)*

**The structural stability of silver (Ag) in dual atmosphere exposure conditions, which are representative of solid oxide fuel cell (SOFC) current collector and gas seals, has been examined in the 600-800 °C temperature range. Experiments conducted on Ag tubular sections exposed to flowing $H_2$-3% $H_2O$ (inside the tube) and air (outside the tube) showed extensive porosity formation along the grain boundaries in the bulk metal. Similar tubular sections, when exposed to air only (both inside and outside the tube), showed no bulk porosity or structural changes. It is postulated that the porosity formation in the bulk metal is related to the formation of gaseous $H_2O$ bubbles due to simultaneous diffusion of hydrogen and oxygen followed by subsequent interaction resulting in the formation of steam. Thermochemical processes that are responsible for structural degradation are presented and discussed. Based on experimental observations, it is concluded that Ag metal may not provide adequate long-term structural stability under a dual-environment condition that is typical of interconnects or gas seals in intermediate temperature SOFCs.**

**Keywords** corrosion, diffusion, hydrogen, silver, solid oxide fuel cell

## 1. Introduction

The solid oxide fuel cell (SOFC), like most solid-state energy conversion devices, operates at high temperatures (600-1000 °C), and produces electricity by electrochemically combining the fuel and oxidant gases across an ionically conducting oxide membrane. To build up a useful voltage, a number of cathode-electrolyte-anode cells are electrically connected in series in a "stack" through bi-polar current collectors/gas separators, also known as interconnects. As the name implies, the interconnect separates the fuel (mixtures of $H_2$, CO, and $CH_x$) at the anode side and at the oxidant (air) at the cathode side, and provides gas flow paths as well as mechanical support for the SOFC stacks. In the bi-polar design, the cell-to-cell interconnects and gas seals remain simultaneously exposed to reducing and oxidizing gas environments. With increased interest in the development of intermediate temperature SOFC systems (650-800 °C) and the use of metallic current collectors, significant interest remains in using silver (Ag) or Ag-based materials for sealing and interconnection.[1-5] For example, Ag has been suggested as an interconnect "electrical contact element" for the construction of bi-polar interconnects.[1] Several Ag-based brazes have also been investigated and recommended as sealing materials to construct the stacks.[2-5] Ag or Ag-based alloys have been studied as potential candidate materials for the electrodes and coatings.[6-8] Literature to date has mostly concentrated on the evaluation of material stability in an oxidizing atmosphere or a reducing environment utilizing appropriate gas mixes.[9] The material performance or the stability under the SOFC bipolar interconnect exposure environments has not been reported.

As a precious metal, Ag possesses good chemical stability, high electrical conductivity, and lower cost than other precious metals such as platinum and gold. Thermodynamic data with oxygen (O) and hydrogen (H) gas dissolution, and their diffusion in Ag have been well documented. Thomas[10] and Siegelin et al.[11] reported that the solubility of H in Ag followed the famous Sievert's law (i.e., the concentration of the dissolved gas species in the solid is proportional to its outside vapor pressure). Katsuta and McLellan[12] and Eichenauer et al.[13] measured the diffusivity of H in solid Ag and determined its activation energy for diffusion. Eichenauer and Muller[14] and Otto[15] studied the dissolution of O in Ag, which indicated that, similar to H, the solubility of O also follows the Sievert's law. Eichenauer and Muller[14] also measured the diffusivity of O in solid Ag at different temperatures. Chalmers et al.[16] first found the faceting or thermal etching of Ag that increased with O content. The surface changes on Ag were attributed to the reconstruction of the crystallographically random surface into low-index planes (usually with low surface energy) such as {100} and {111} via surface diffusion,[16-18] and the formation of unstable $Ag_2O$ that may subsequently vaporize and deposit onto the low index areas on the surface.[19] The thermal etching or erosion leads to a weight loss of Ag, which increases with the airflow rate. However, studies also have indicated that no structural changes of the Ag on the surface were observed in a

This paper was presented at the Fuel Cells: Materials, Processing, and Manufacturing Technologies Symposium sponsored by the Energy/Utilities Industrial Sector & Ground Transportation Industrial Sector and the Specialty Materials Critical Technologies Sector at the ASM International Materials Solutions Conference, October 13-15, 2003, in Pittsburgh, PA. The symposium was organized by P. Singh, Pacific Northwest National Laboratory, S.C. Deevi, Philip Morris USA, T. Armstrong, Oak Ridge National Laboratory, and T. Dubois, U.S. Army CECOM.

**Prabhakar Singh, Zhenguo Yang, Vish Viswanathan,** and **Jeff W. Stevenson,** Pacific Northwest National Laboratory, Richland, WA 99352. Contact e-mail: prabhakar.singh@pnl.gov.

reducing atmosphere,[1] and thermal etching was effectively mitigated in static air or in a closed system.[19]

In the 1960s, Klueh and Mullins[9] investigated the H-induced embrittlement of Ag. In their work, both single and polycrystalline Ag samples were annealed in a partial pressure of O until saturation and then were heat-treated in a partial pressure of H. It was found that H diffused into Ag and reacted with the dissolved O, resulting in the precipitation of water bubbles. The bubbles that formed in the single crystal Ag led to the formation of large blisters and cracks, and when polycrystalline specimens were used, grain boundary cracking was observed.

In this work, the structural stability of Ag under dual-environment exposure conditions that simulate current collector and gas seal applications in SOFCs is examined and presented.

## 2. Experimental

The experimental setup used during this study is schematically shown in Fig. 1. Two 6.35 mm (1/4 inch) outside diameter identical Ag (99.9%) tubular samples with a wall thickness of 0.25 mm were held in a vertical, tubular furnace. Gas flow arrangements included flowing $H_2$-3% $H_2O$ (obtained by bubbling dry $H_2$ through a water bubbler maintained at room temperature) at a rate of 10 $cm^3$/min through one Ag tube with the outside surface exposed to ambient air. The second Ag tube remained exposed to the flowing ambient air at both the inside and outside surfaces of the tube. The furnace was heated to the designated temperature at a rate of 2 °C/min and was held there for 100 h, followed by cooling to room temperature at the same rate as that upon heating. A series of stability tests were carried out at 700 °C, 600 °C, and 500 °C, respectively.

After the furnace was cooled down to room temperature, the Ag tubes were removed from the furnace for visual and microscopic evaluation. Both optical and scanning electron microscope (SEM) analyses were performed on the surface at selected locations, including the fracture surface if the tube had been broken during the test. The tube samples were then cut into sections that were subsequently mounted and carefully polished. Both fractured and polished sections were analyzed using the aforementioned techniques.

## 3. Results

Ag tubular section exposed to 700 °C and the dual-atmosphere condition (i.e., flowing $H_2$-3% $H_2O$ on the inside and air on the outside surface of the tube wall) showed cracking after 100 h (Fig. 2). Under the light-stereo microscope, tube sections also showed deformation and blisters. The tube exposed to air on both the inside and outside, however, remained shiny and did not show any indication of cracking. The SEM observation of the fracture surface of the broken tube indicated that the solid Ag metal had completely disintegrated during the testing, as shown in Fig. 3(a). The further enlarged image in Fig. 3(b) revealed that the Ag was full of voids and was thermally etched or eroded severely. Away from the fracture site (marked as "B" in Fig. 2), cracks and fissures were clearly visible, as shown in Fig. 3(c). The enlarged image in Fig. 3(d) revealed that these cracks and fissures nucleated and propagated along grain boundaries. The enlarged image from the site (marked as "c" in Fig. 3e) is shown in Fig. 3(f), and clearly illustrates plastic deformation and the early stage of nucleation and growth of cracks along grain boundaries. Besides the outside wall of the Ag tube, the inside wall was also examined. A typical SEM image of the inside wall in the section of the hot zone is shown in Fig. 4, where the thermal etching or erosion and crystal facets are clearly visible.

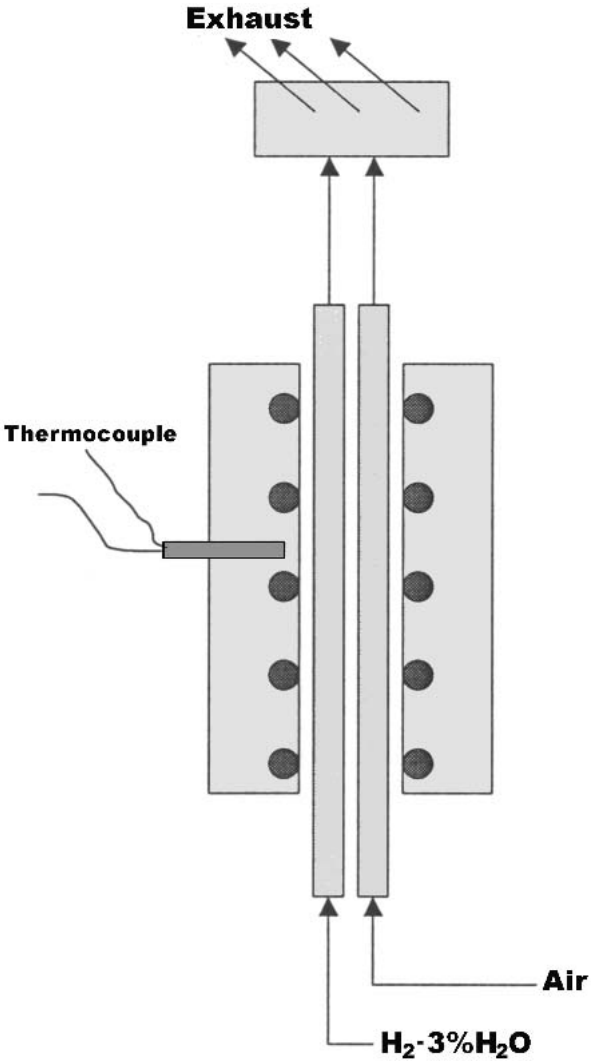


**Fig. 1** The scheme of experimental arrangement

The Ag tube, exposed to air only, showed a smooth surface without cracks or voids, as shown in Fig. 5(a). The enlarged images of the surface are shown in Fig. 5(b) and (c). Evidence of thermal etching is evident on the surface and the grain boundaries.

Sections of Ag tubes were subsequently sectioned, polished, and analyzed using light and scanning electron microscopy. Figure 6 shows microstructures of the cross-sectioned tube walls. It can be seen that for the tube with ($H_2$ + 3% $H_2O$) flow, the inner walls were full of voids or pores, with a number of cracks penetrating the surface. Direct observation of the cross sections of the tube wall, as shown in Fig. 7(a) and (b), indicated that the porosity formed within the metal wall remained

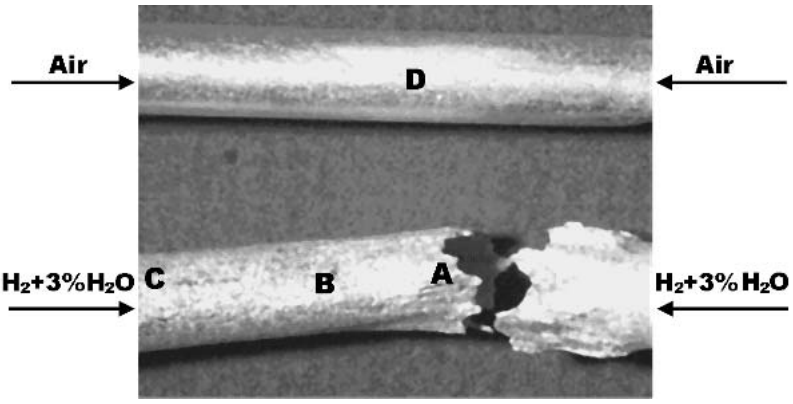


**Fig. 2** The light-stereo microscopic picture of tubular samples after 100 hours of heat-treating at 700 °C with flow of air and wet H inside, respectively.

interconnected. In comparison, the cross-section of the tube exposed to the ambient air was still fully dense without voids or pores.

As the temperature was decreased to 600 °C, the tube with the flow of $H_2$ + 3% $H_2O$ during heating was not completely broken after 100 h of operation (Fig. 8), however, plastic deformation, open cracks, and fissures were still visible. With further reduction in temperature to 500 °C, no open cracks and fissures were observed on the Ag wall in the hot zone after 100 h. The microscopic observation on the cross sections of these two tubes with flowing of $H_2$ + 3% $H_2O$, as shown in Fig. 9(a) and (b), respectively, indicated that porosity developed in the bulk Ag at both 600 °C and 500 °C. The population of pores decreased with decreasing exposure temperature. Besides the population density of the pores, the size of the pores and cracks also decreased at lower exposure temperatures. In contrast to the tube with flowing $H_2$ + 3% $H_2O$ during heating, no structural degradation due to the formation of porosity was noticed on the samples which were exposed to air both inside and outside during heating at these two temperatures.

## 4. Discussion

### 4.1 Structural Degradation and Bubble Formation

Pore formation within the solid Ag is postulated to be due to the dissolution of gaseous molecules in the metal followed by reaction of the dissolved gas species to form $H_2O$ molecules (i.e., water vapor). Water bubble formation is schematically shown in Fig. 10. It starts with the adsorption of gaseous molecules, with subsequent dissociation and dissolution of H and O gases on the inside and outside walls of the Ag tube. The dissociated H and O atoms diffuse into the Ag lattice favorably via fast diffusion paths such as grain boundaries and dislocations. Both H and O diffuse significantly faster in the solid Ag at elevated temperatures. For example, at 700 °C the diffusivities of H and O in solid Ag are $2.17 \times 10^{-4}$ $cm^2/s$,[12] and $9.26 \times 10^{-5}$ $cm^2/s$,[14] respectively, which are equivalent to 1 h diffusion distances of 8.8 mm for H and 5.9 mm for O. In other words, H and O can penetrate the wall of the Ag tube in less than 1 h at 700 °C. Along with diffusion, H and O atoms can be trapped at interstitial or defect sites, increasing their concentration. This process is governed by Sievert's law (i.e., the concentration of dissolved gas species in the solid is proportional to its vapor pressure).

With continuous build-up and further penetration, H and O combine to form water vapor in the solid. The reaction is most likely initiated at defect sites, such as grain boundaries, where the crystal lattice is discontinuous, and inhomogeneous nucleation is thermodynamically favorable. It is believed that in the early stages of the reaction, the surface tension restrains the pressure of the water vapor.[11] With the growth of bubbles, the restraint is distributed between the surface forces and the creep strength of Ag, leading eventually to all of the restraint being provided by the strength of metal. At a certain stage, the pressure of water vapor exceeds the mechanical strength of Ag, resulting in gross plastic deformation and fracture at the crack tip where the stress is concentrated. Thus, the growth of water bubbles is realized, and, as observed, blisters are generated on the surface of the Ag. With continued growth, water bubbles tend to impinge, leading to the formation of fissures and cracks. If a pore of water vapor nucleates and grows just beneath the surface, it might escape, leaving a hole, which has been confirmed by surface microstructure analysis (refer to Fig. 3).

### 4.2 Thermodynamic Modeling of Water Phase Formation

As discussed earlier, porosity in Ag during exposure to H and air is attributed to the formation of water bubbles as a result of the reaction between dissolved H and O in the solid Ag at elevated temperatures:

$$2[H]_{Ag} + [O]_{Ag} = H_2O(g) \quad \text{(Eq 1)}$$

The water vapor partial pressure can be expressed as

$$\mathrm{Log}P_{H_2O} = -\frac{\Delta G^o}{4.57T} + 2\log a_{[H]} + \log a_{[O]} \quad \text{(Eq 2)}$$

where $\Delta G^o$ is obtained from published thermodynamic data.[20] Since the equilibrium concentration of dissolved vapor species is low, the Ag solid solution can be considered an infinite dilute solution. Thus, the activities in Eq 2 are replaced by concentrations, leading to

$$\mathrm{Log}P_{H_2O} = -\frac{\Delta G^o}{4.57T} + 2\log c_{[H]} + \log c_{[O]} \quad \text{(Eq 3)}$$

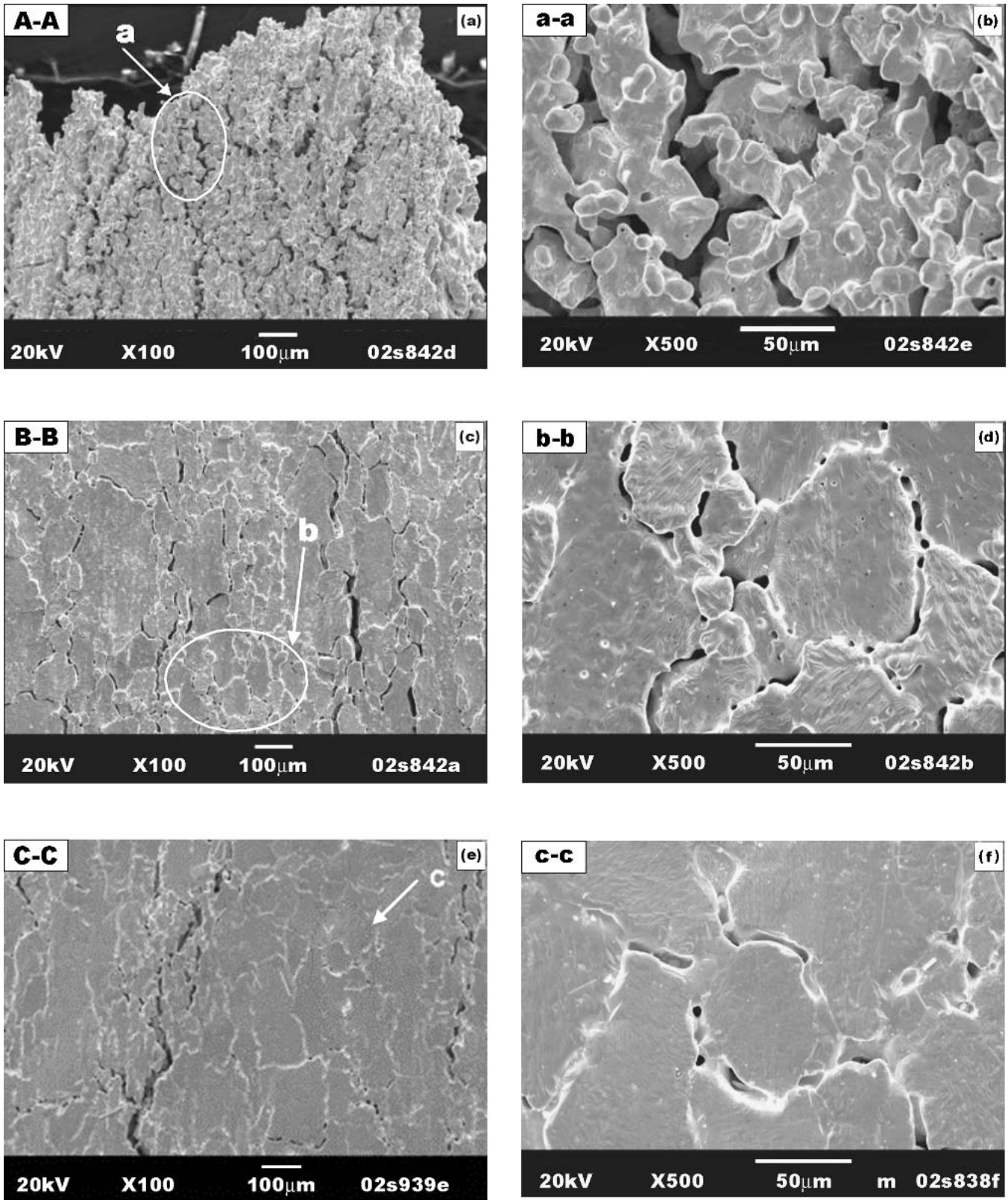


**Fig. 3** Second electron SEM images of the tube after 100 h of heat treatment at 700 °C with flow of ($H_2$ + 3% $H_2O$) during heating: (**a**) a microstructure of the fracture surface at a site marked as "A"in Fig. 2; (**b**) the enlarged one at site "a" in (a); (**c**) a surface microstructure from the site marked as "B" in Fig. 2; (**d**) the enlarged one at site "b" in (c); (**e**) a surface microstructure from the site marked as "C" in Fig. 2; and (**f**) the enlarged one at site "c" in (e)

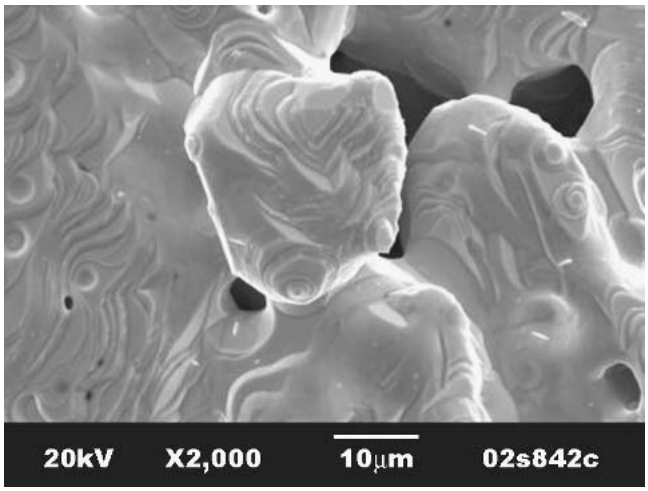


**Fig. 4** A surface SEM image of the inner wall of the Ag tube in the hot zone, after 100 h of heat treatment at 700 °C with flow of ($H_2$ + 3% $H_2O$) during heating

According to data published for H and O in the solid Ag,[10,14] the partial pressure of water vapor formed via the reaction of dissolved H and O can be expressed as a function of temperature, O, and H vapor pressure as follows:

$$\mathrm{Log}P_{H_2O} = -\frac{(\Delta G^{o} + 44{,}740.3)}{4.57T} - 3.93 + \log P_{H_2} + \frac{1}{2}\log P_{O_2} \quad \text{(Eq 4)}$$

The equilibrium partial pressure is shown in Fig. 11 as a function of temperature at different H partial pressures. It can be seen that from room temperature to the melting point of Ag, thermodynamic modeling predicts a high partial pressure of water vapor, which increases with decreasing temperature. At 700 °C calculations indicate a partial pressure of $10^{11.07}$ atm, with wet H (97% $H_2$ + 3% $H_2O$) on one side and air (21% $O_2$) on the other (i.e., under current test conditions). Thus, the reaction of dissolved H and O in solid Ag to yield water vapor

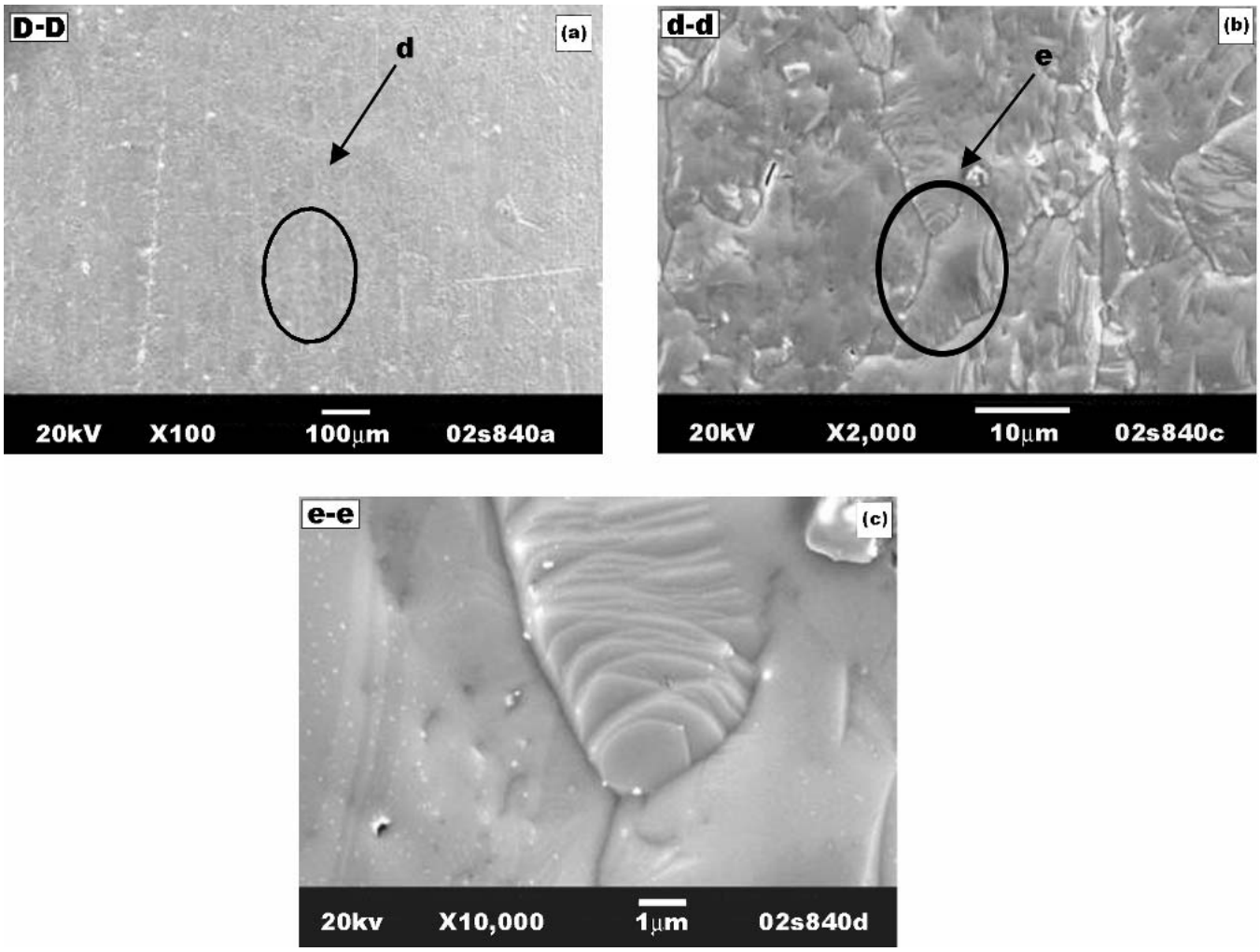


**Fig. 5** Surface SEM images of the tube after 100 h of heat treatment at 700 °C with a flow of air both inside and outside during heating: (**a**) a surface microstructure from the site marked as "D" in Fig. 2, the enlarged one from the site marked as "d" in (a), and the further enlarged one from the site marked as "e" in (**b**)

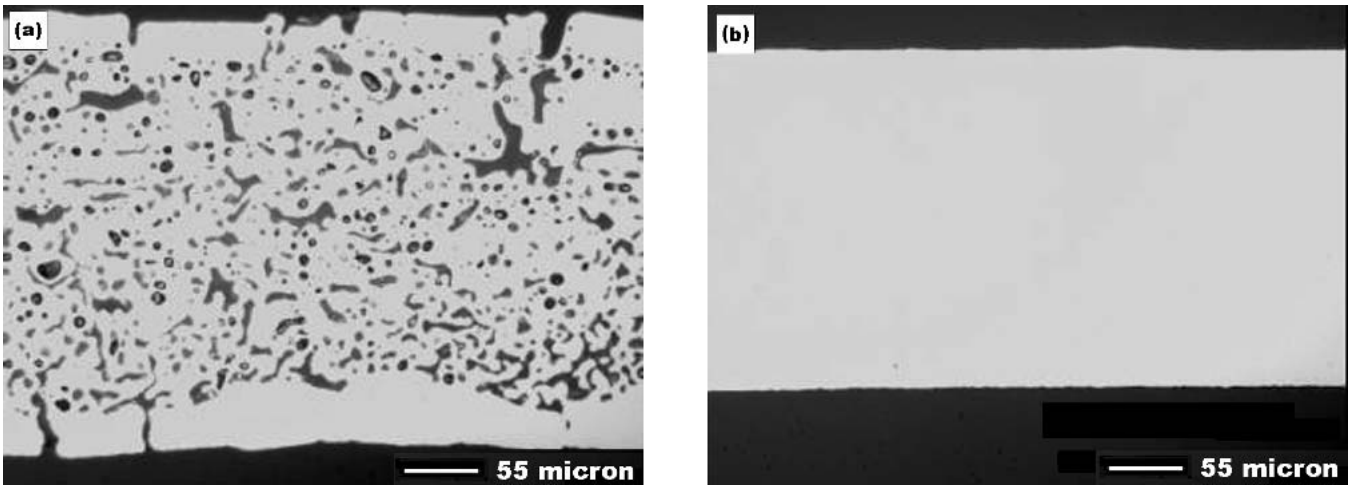


**Fig. 6** Microstructures of cross sections of tube wall: (**a**) with flow of ($H_2$ + 3% $H_2O$); and (**b**) with flow of air

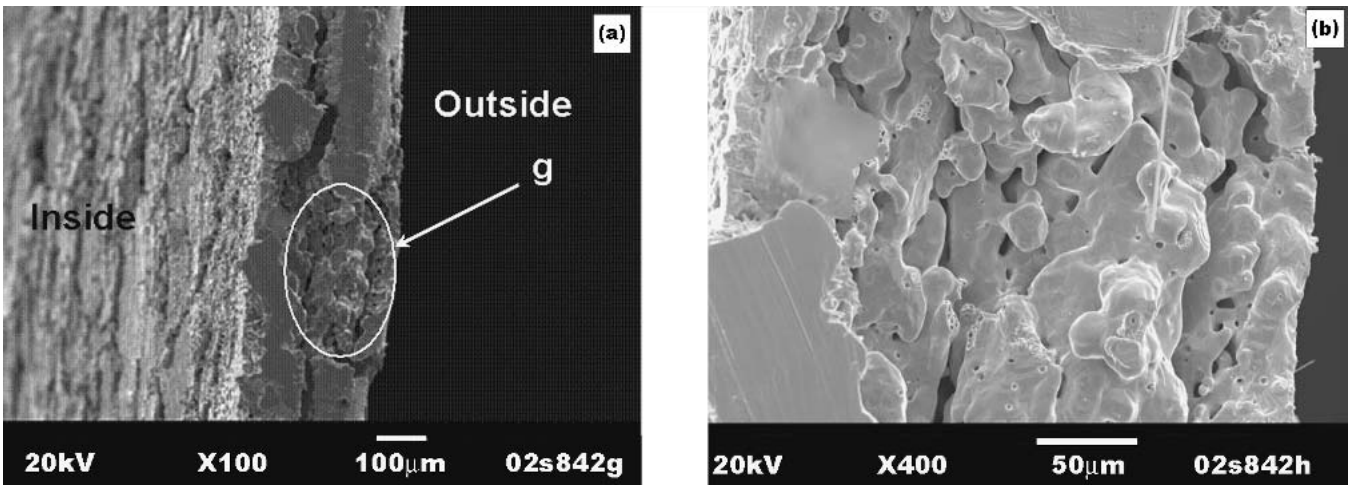


**Fig. 7** SEM images of the cross sections of the tube wall after 100 h of heat treatment at 700 °C with a flow of air both inside and outside during heating

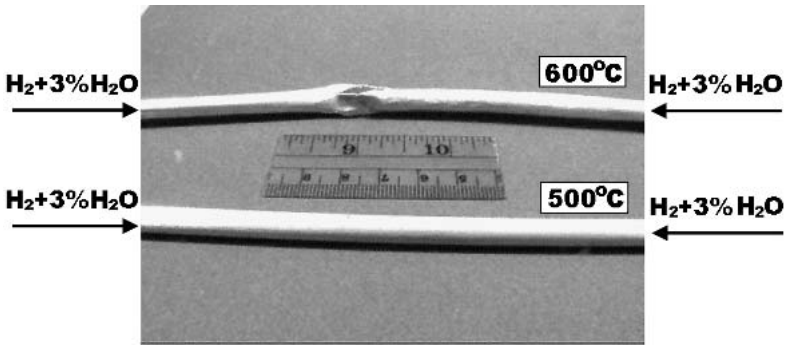


**Fig. 8** The light-stereo microscopic pictures of tubular samples after 100 h of heat-treating with a flow of wet H inside at 600 °C and 500 °C, respectively

is thermodynamically highly favorable. In addition, calculations also indicate that a higher partial pressure of H makes high-pressure steam bubble formation thermodynamically more favorable in solid Ag. It should be pointed out, however, that kinetics have not been considered in this modeling. At low temperatures, the sorption process and the transport of dis-

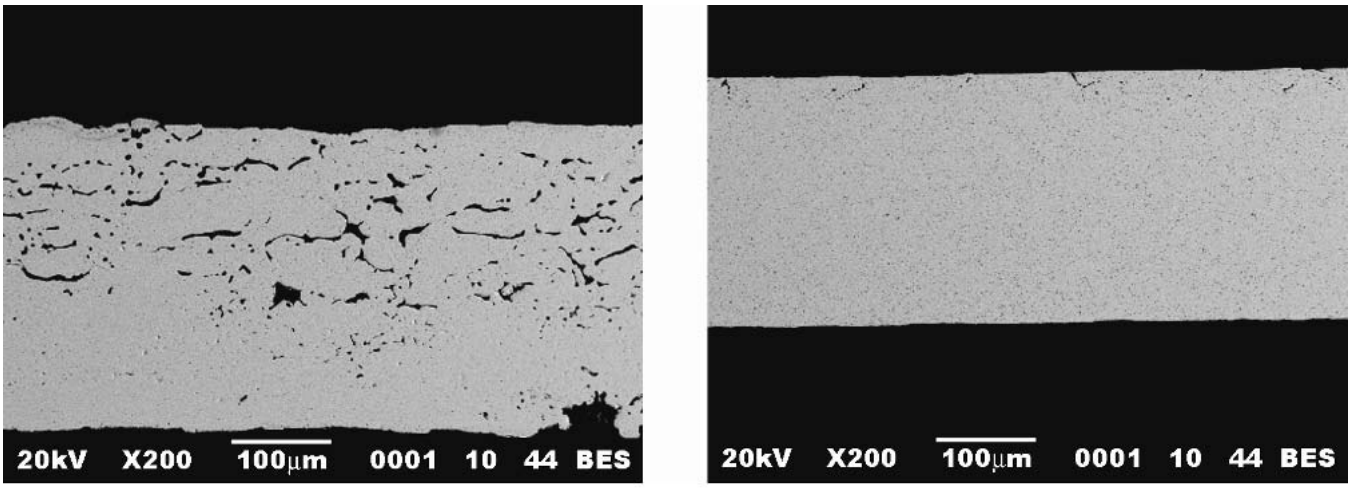


(a) (b)

**Fig. 9** Microstructures of cross sections of tube wall after pre-heat treatment of 100 h with a flow of ($H_2$ + 3% $H_2O$) at (**a**) 600 °C and (**b**) 500 °C, respectively

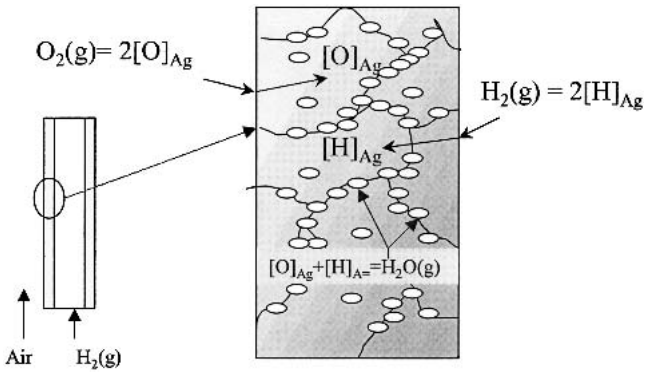


**Fig. 10** Schematic of degradation process and reaction steps

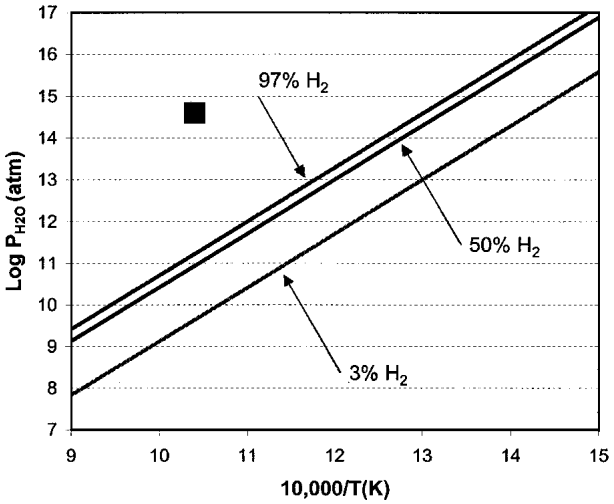


**Fig. 11** Water vapor partial pressure as a function of temperature at different concentrations of H gas

solved species in the Ag may become dominant factors, affecting the reaction rate of water phase formation.

## 5. Conclusions

As found in this study, the simultaneous exposure of Ag to a reducing and an oxidizing environment leads to extensive pore development in bulk Ag at elevated temperatures that can be as low as 500 °C. Pore formation takes place predominantly along the grain boundary. The formation of water vapor is attributed to the nucleation and growth of high-pressure steam bubbles that connect to form the pores and fissures in the Ag. The water evolves as high-pressure steam, and is related to the high solubility and fast diffusivity of H and O in the Ag. Thermodynamic modeling indicates that the following reaction is highly favorable:

$$2[H]_{Ag} + [O]_{Ag} = H_2O(g) \quad \text{(Eq 5)}$$

The extensive formation of pores and cracks in the Ag wall exposed to the dual air-$H_2$-3% $H_2O$ environment will have an obvious impact on its long-term structural stability. Such degradation can result in the development of leaks and the resultant mixing of fuel and oxidant in SOFCs. Thus, it will be difficult for Ag or Ag-based alloys to be used as components in fabricating current collector or gas seals that are exposed to a dual atmosphere.

### Acknowledgments

The authors would like to thank Nat Saenz, Shelly Carlson, Guanguang Xia, and Jim Coleman for their assistance in metallographic and SEM sample preparation and analysis. The work summarized in this article was funded as part of the Solid-State Energy Conversion Alliance (SECA) Core Technology Program by the National Energy Technology Laboratory (NETL) of the US Department of Energy. Pacific Northwest National Laboratory is operated by Battelle Memorial Institute for the

US Department of Energy under contract DE-AC06-76RLO 1830.

## References


1. W.A. Meulenberg, O. Teller, U. Flesch, H.P. Buchkremer, and D.J. Stover: "Improved Contacting by the Use of Silver in Solid Oxide Fuel Cells Up to an Operating Temperature of 800 °C," *J. Mater. Sci. Eng.*, 2001, *36*, pp. 3189-95.
2. Y. Harufuji: Japan Patent 06231784 (1994).
3. Y. Harufuji and S. Yoshida: Japan Patent 06084530 (1994).
4. A.V. Virkar, W.D. Prouse, P.C. Smith, and G.Y. Lin: US Patent 2002048700 (2002).
5. K.S. Weil and D.M. Paxton: "Development of An Oxidation Resistant Ceramic-to-Metal Braze for Use in YSZ-Based Electrochemical Devices," *Ceram. Eng. Sci. Proc.*, 2002, *23*, pp. 785-92.
6. X. Xiao, C.Q. Tang, and Z.C. Xia: "Solid Oxide Fuel Cells With Different Cathode Materials," *Dianyuan Jishu*, 2002, *26*, pp. 128-30.
7. A.Q. Pham, B.W. Chung, and R.S. Glass: US Patent 2002127460 (2002).
8. U.D. Diekmann, H. Goebbels, and E. Sigismund: DE 2002014011 (2002).
9. R.L. Klueh and W.W. Mullins: "Some Observations on Hydrogen Embrittlement of Silver," *Trans. Met. Soc.*, 1968, *242*, pp. 237-44.
10. G.L. Thomas:"Solubility of Hydrogen in Solid Copper, Silver, and Gold Obtained by a Rapid Quench and Extraction Technique," *Trans. AIME*, 1967, *239*, pp. 485-90.
11. W. Siegelin, K.H. Lieser, and H. Witte: *Z. Elektrochem.*, 1957, *61*, pp. 359-66.
12. H. Katsuta and R.B. McLellan: "Diffusivity of Hydrogen in Silver," *Scripta Metall.*, 1979, *13*, pp. 65-66.
13. W. Eichenauer, H. Kunzig, and A.Z. Pebler: *Metallkde*, 1958, *49*, pp. 220-25.
14. W. Eichenauer and G. Muller: *Z. Metallkde*, 1962, *53*, pp. 321-25.
15. E.M. Otto: "Equilibrium Pressure of Oxygen Over Ag-O-Ag at Various Temperatures," *J. Electrochem. Soc.*, 1966, *113*, pp. 643-45.
16. B. Chalmers, R. King, and R. Shuttleworth: *Proc. R. Soc.*, 1948, *A193*, p. 465.
17. T.C. Wei and J. Philips: *Adv. Catal.*, 1996, *41*, p. 359.
18. X. Bao, G. Lehmpfuhl, G. Weinberg, R. Schlogl, and G. Ertl: *J. Chem. Soc. Faraday Trans.*, 1992, *88*, p. 865.
19. E.D. Hondros and A.J.W. Moore: "Evaporation and Thermal Etching," *Acta Metall.*, 1960, *8*, pp. 647-53.
20. E. Fromm and E. Gebhardt: *Gase und Kohlenstoff in Metallen*, Springer-Verlag, Berlin/Heidelberg, 1976.